

Fully porous GaN p-n junctions fabricated by Chemical Vapor Deposition: a green technology towards more efficient LEDs

J. J. Carvajal^a, J. Mena^a, O. V. Bilousov^a, O. Martínez^b, J. Jiménez^b, V. Zubialevich^c, P. Parbrook^{c,d}, H. Geaney^{c,e}, C.O'Dwyer^{c,e}, F. Díaz^a and M. Aguiló^a

^a Física i Cristal·lografia de Materials i Nanomaterials (FiCMA-FiCNA) and EMaS, Universitat Rovira i Virgili (URV), Marcel·lí Domingo, 1, E-43007, Spain

^b GdS-Optronlab, Departamento de Física Materia Condensada, Univ. de Valladolid, Edificio I+D, Paseo de Belén, 11, 47011, Valladolid, Spain

^c Tyndall National Institute, Lee Maltings, Dyke Parade, Cork, Ireland

^d School of Engineering, University College Cork, Cork, Ireland

^e Department of Chemistry, University College Cork, Cork, Ireland

Porous GaN based LEDs produced by corrosion etching techniques demonstrated enhanced light extraction efficiency in the past. However, these fabrication techniques require further postgrown processing steps, which increase the price of the final system. In this paper, we review the process followed towards the fabrication of fully porous GaN *p-n* junctions directly during the growth step, using a sequential chemical vapor deposition (CVD) process to produce the different layers that form the *p-n* junction.

Introduction

The discovery of light-emitting porous Si (1) propelled investigations of porosity formation in semiconductors (2-4). Porous semiconductors have received a considerable interest, primarily due to their unusual optical and electrical properties, that sometimes can be radically different from those of the bulk material. Here we should consider not only basic semiconductor parameters like conductivity, band gap energy and absorption/emission of light, which might be quite different, but also internal symmetries/anisotropies, high-order effects and even basic chemistry. Some of the novel properties discovered for porous semiconductors are: (i) fast chemical reactions, practically not previously observed in bulk materials, including violent explosions due to the large surface to volume ratio and optical diffusion conditions (5); (ii) novel absorption characteristics (e.g., transparent for UV while blocking larger wavelengths) (6); (iii) optical anisotropy (7), and new types of optical anisotropy not encountered in natural materials if two or more sets of pores are present simultaneously (8); (iv) strongly decreased thermal conductivity (and concomitantly changed phonon spectra) (9); (v) strongly changed the electrical conductivity, sensitive to the presence of gases or humidity (10), among others.

The recent advances in the production technologies of porous semiconductor materials together with the unique properties that these materials exhibit have promoted its utilization in the fabrication of devices for advanced nanoelectronics, sensors with enhanced sensitivity, interfacial structures and catalysis, among others (11). Actually, the

applications of these materials depend on the development of processing methods able to precisely control the optical and electrical properties of the resulting porous materials.

Among porous semiconductor materials, wide band gap semiconductors, and in particular, porous GaN, play an important role in the development of new technologies for applications in optoelectronics, magnetism, catalysis and biotechnology.

Nowadays, GaN is considered one of the most important semiconductors for a number of applications in electronics and optoelectronics, principally due to its wide direct band gap (3.39 eV at room temperature) (12). It has also excellent prospects for high temperature electronics because of its large band gap, high thermal stability and excellent physical properties (13). On the other hand, GaN also has high heat capacity and thermal conductivity (14-16) making it suitable for high power and high frequency applications. Furthermore, GaN can withstand ionizing radiations better than other semiconductor materials, which makes of GaN a good option for space, betavoltaics and photovoltaics use (17,18). GaN crystallizes in the hexagonal system with the space group $P6_3mc$ (wurtzite structure) (19). GaN-based laser diodes are used to read blue-ray discs; GaN high-electron-mobility transistors (HEMTs) are used in various wireless infrastructures; GaN-based metal-oxide-semiconductor and metal-semiconductor field-effect transistors (MOSFET and MESFET, respectively) offer many advantages in high power electronics for automotive applications. However, the most important application of GaN is found in light emitting diodes (LEDs) as the active light emitting element of various optical components, ranging from traffic lights to large area displays.

In its porous form, GaN has received particular interest in the last decade due to interesting optical and electronic properties that allowed, for instance, the demonstration of gas sensors with enhanced sensitivity and also LEDs with improved light extraction efficiency, of crucial importance for the modern society, since a significant amount of energy consumed is used for lighting. Porous GaN exhibits some interesting specific properties. A strong photoresponse was observed in epitaxial GaN layers grown on 6H-SiC substrates and anodized in aqueous solutions of HF (20). It has been proved that porous GaN exhibited lower stress compared to its bulk counterpart (21). In some cases it has been observed that porous GaN shifts its band edge emission further into the UV due to quantum confinement, which appears due to wire-like structures in porous GaN (22). Finally, it has been reported that photoluminescence (PL) intensity in porous GaN increases with respect to its bulk counterpart (23).

Porous GaN has been typically fabricated by (photo) electrochemical etching and chemical etching methods. For instance, porous GaN has been produced by anodic etching (24) using a 0.1 M NaOH solution with 0.2 M NaCl, a Pt electrode as the cathode and GaN as the anode, and a DC voltage supply that provides constant current between the electrodes through the NaOH electrolyte, obtaining the whole area of the GaN film covered by pores after the etching process. Porous GaN has also been produced by Pt-assisted electroless etching (25), which does not require any external voltage or electrical contact, by immersing a Pt-coated GaN substrate in a solution of methanol, HF and hydrogen peroxide in a 1:2:1 volume ratio, and illuminating it with a mercury lamp to enhance the process. In that case, the morphology is dominated by the formation of ridge-like structures evolving over the etching time, forming a deep porous network in between and under the ridges. UV-assisted photo-electrochemical wet etching has also been used to produce porous GaN (23,26) using a buffered HF aqueous solution (HF:H₂O = 2:1, volume ratio) as electrolyte, a Pt electrode as the cathode and GaN as the anode. Another way of producing porous GaN has been the use of an alternating current photo-assisted electrochemical etching (22) in a 4 wt % KOH electrolyte under UV illumination and

with a 50 Hz sine-wave AC current, using a Pt electrode and GaN as the cathode and anode respectively. This technique allowed obtaining well-defined layers of hexagonal like pores of GaN with sizes that increased with the etching time, and depending on the quality of the starting GaN epilayers.

The (electro)chemical reactions are sensitive to many parameters, such as the electrolyte chemistry, applied potential or current density, temperature, electrolyte flow conditions, doping type, and doping concentration of the semiconductor, illumination, and surface conditions (polished, rough, masked). These limitations, together with the complex equipment required to control each parameter, and the fact that many electrolytes are highly toxic and/or corrosive, makes the production process from a technical point of view challenging.

Despite all these limitations, porous GaN has been used for a wide range of applications. For instance, porous GaN thin films have been used as buffer layers in growing epitaxial GaN layers with a lower level of defects (28), or in a lift-off process of GaN and devices through an electrochemical anodization process to generate a voided region with decreased lateral fracture resistance (29). Porous GaN has also been used to fabricate Schottky diode gas sensors for hydrogen detection with high sensitivity (30,31). Porosity in GaN has also been used to enhance the light extraction and internal quantum efficiencies of GaN-based LEDs (32-40).

Nevertheless, it is worth to explore new production techniques for porous GaN that overcome the limitations listed above, and if possible, simplify the synthesis processes. In this context, we have been able to produce porous GaN through the direct reaction of metallic Ga with NH_3 in a simple chemical vapor deposition (CVD) system that does not require any secondary electrochemical or electroless etching, nor subsequent chemical treatment after growth to induce the porosity (41,42). This approach is simpler and cheaper than the preexisting technologies. Also, it does not use corrosive electrolytes or toxic metallorganic compounds, allowing for the generation of a green technology for the production of porous GaN. This technique allowed us the production of micrometer sized nanoporous GaN particles onto BN substrates (41) or the deposition of porous GaN directly onto Si substrates in a single growth step (42). This motivated us to investigate the possibility of developing new electronic and optoelectronic devices with improved external quantum efficiencies, the incorporation of phosphors for LEDs, and high surface area sensing.

Here, we report a summary of the most important achievements obtained in this field, namely the epitaxial growth of *n*-type and *p*-type porous GaN thin films on non-porous GaN substrates to fabricate functional porous GaN *p-n* junctions.

Results and Discussion

Influence of the substrate on the texturation of porous GaN films

Different substrates were investigated to ascertain if they might play a role in the crystallographic orientation of the porous GaN particles. In a first attempt we used different substrates, e.g. amorphous SiO_2 (fused silica), tungsten wire, (111) silicon, and pyrolytic boron nitride (p-BN). We have chosen these substrates with the criterion of using an amorphous substrate (fused silica), a cubic substrate different than Si and without a particular crystallographic orientation (W wire), and a substrate with hexagonal structure (p-BN). We also tested (111) Si since it has been reported that (0001) GaN films can be deposited on these substrates (43). Since this is the direction along which the pores

of GaN are aligned (44), it can provide a way to orient the porous GaN particles. In all cases, with the exception of (111) Si, we sprayed an ethanolic solution of $\text{Ni}(\text{NO}_3)_2$ on the surface of the substrates to facilitate the nucleation of GaN. (111) Si substrates were coated with 20 nm thick films of Au, Pt, Ti or W, used as catalysts for the growth of porous GaN.

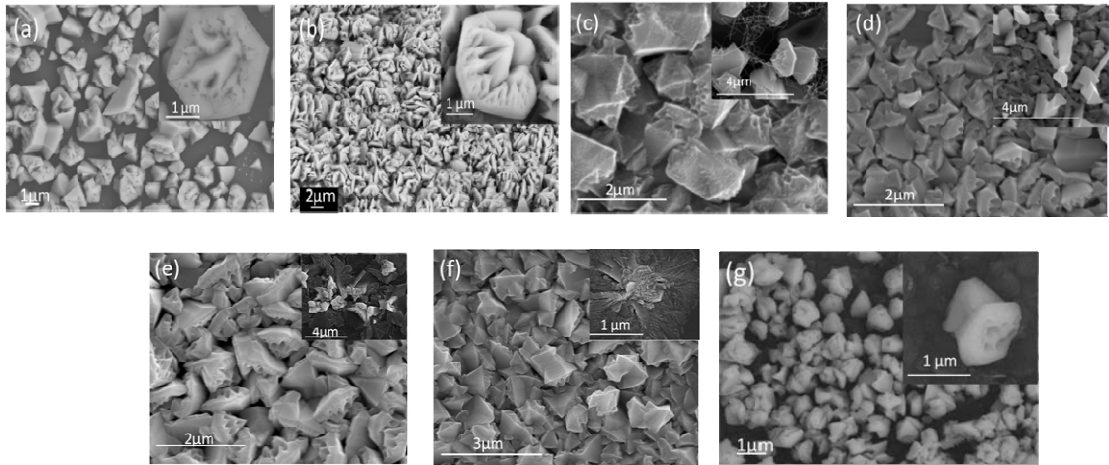


Figure 1. SEM images of the nanoporous GaN particles grown on different substrates: (a) amorphous SiO_2 (fused silica), (b) W wire, (c-f) (111) Si coated with different catalysts (c) Au, (d) Pt, (e) Ti and (f) W and (g) pyrolytic BN.

SEM pictures of the nanoporous GaN particles grown on these substrates reveal in all cases that GaN appears in the form of hexagonal micron-sized nanoporous particles (see Figure 1). When using fused silica, the particles present low porosity, with the pores more concentrated at the central part of the particles, and with elongated shape towards the external parts of the particles (see Figure 1(a)). On the W wire, the density of micron-sized nanoporous particles is very high (see Figure 1(b)). Meanwhile, GaN grown on (111) Si substrates coated with different catalyst appears presents micron-sized nanoporous particles with a mean particle size of 2-5 μm (see Figures 1 (c-f)). The lowest porosity was obtained when W was used as catalyst (see Figure 1 (f)). In most of the cases, nanowires were also observed together with the porous particles, especially when Au and Pt were used as catalyst (see insets in Figures 1 (c-d)). When Ti and W were used as a catalysts, apparently an early stage of epitaxial growth is observed at the edges of the samples (see insets in Figures 1 (e-f)), but it fades away in the center of the sample where we a higher density of particles is observed. According to these images it seems that the combination of the substrate and the catalysts plays a relevant role in the morphology of the particles. Finally, in the case of p-BN, a certain degree of alignment of the GaN particles can be observed, since a bigger number of pores perpendicular to the surface can be seen (Figure 1 (g)); however, due to the misalignment of the BN flakes that form the p-BN substrate, there are also particles with different crystallographic orientations. Also, the porosity degree in these particles is lower than in the other cases.

, The XRD characterization of these samples, as expected from the SEM pictures, did not reveal any preferential growth along any particular direction, with the exception of those grown on a (111) Si substrate coated with Ti and W,. This might be related to the fact that the interlayer formed by the catalysts, located between the substrate and the GaN

layer, hinders the influence that the structure of the substrate has on the growing GaN layer. In the case of the porous layers grown on (111) Si substrates coated with Ti and W, XRD characterization reveals an incipient degree of texturation of the films, as confirmed by the non-uniform distribution of the intensity in the Debye rings observed with the GADDS detector (see Figure 2), and the different intensity of the diffraction peaks when compared to the reference XRD pattern for GaN (00-050-0792 JCPDS file) included in Figure 2 (c) for comparison. This is more evident when we compare this XRD pattern with any of those recorded for the porous GaN particles obtained using other catalysts. The results for a (111) Si substrate coated with $\text{Ni}(\text{NO}_3)_2$ are included in the figure to visualize this effect. However, it is not an easy task to determine the preferential orientation of the particles, from the data obtained, since the decrease in intensity is observed for diffraction peaks with components in all crystallographic directions. A closer look to the intensity of the peaks seems to indicate that those that have a component along the *c* crystallographic direction tend to decrease in intensity, which would indicate that the preferential orientation of the particles is perpendicular to this direction. In fact, the peak that shows a relative intensity corresponding to what was expected from the reference pattern is the one corresponding to the (11-20) plane, which would indicate that the preferential orientation should be along the [11-20] direction or a combination of components in the *a* and *b* crystallographic directions. However, we could not record other diffraction peaks of the family of planes to confirm this hypothesis.

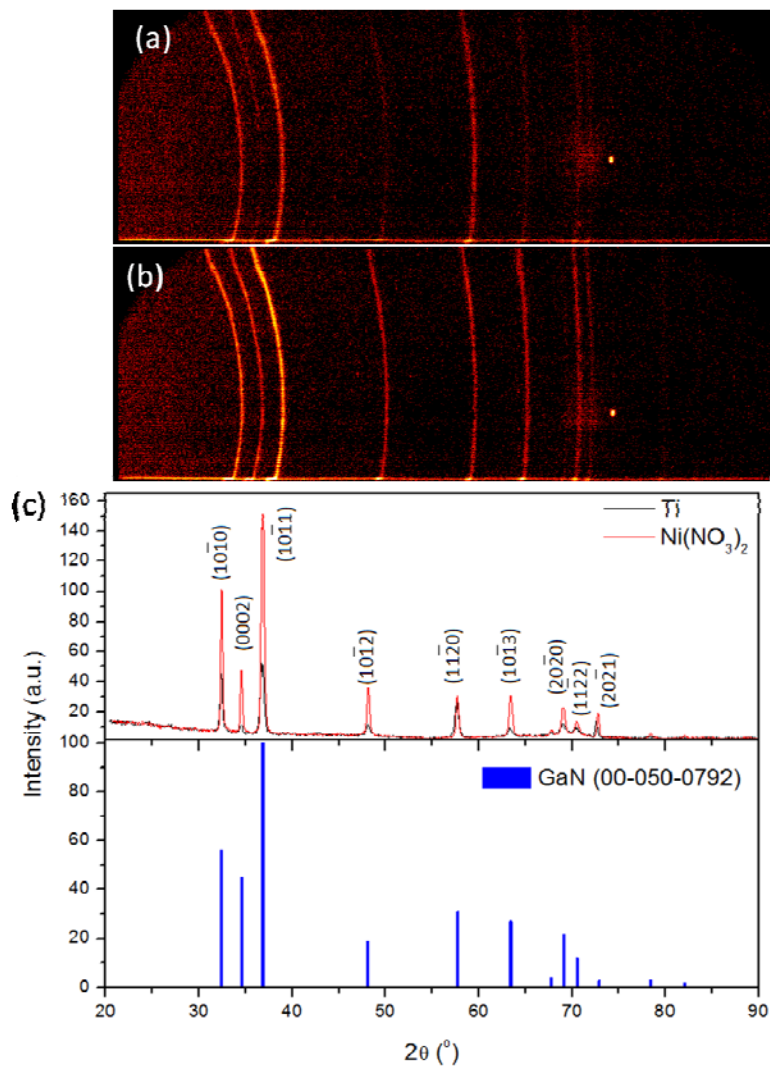


Figure 2. X-ray diffraction patterns of nanoporous GaN obtained on (111) Si substrates coated with Ti and Ni(NO₃)₂. (a,b) Debye rings recorded for both samples, respectively, and (c) diffraction patterns. The reference pattern of GaN from JCPDS (00-050-0792) has been included for comparison.

Chemical Vapor Deposition on patterned (111) Si substrates

This incipient texturation observed in some of the samples obtained on (111) substrates coated with Ti and W, encouraged us to follow this idea of crystallographic orientation of the porous GaN particles. The next step was to use patterned (111) Si substrates (to reduce the number of nanoporous GaN particles nucleating on the surface of the substrate) coated with Ti, to analyze the possible extension of the texturation of the sample. The use of Ti as a catalysts was motivated by previous studies showing that Ti can act as a pre-orienting layer for the deposition of GaN on glass substrates for LEDs applications, since Ti has the same hexagonal crystal lattice structure as GaN with a relative small lattice mismatch ($\Delta a/a = 7.4\%$) (45).

We used commercial (111) Si wafers coated with a thermally grown SiO₂ thin layer, 50 nm thick. The SiO₂ layer was patterned with a 2D array of holes, 1.5 μm in diameter,

using laser lithography and etching techniques. Metallic Ti was deposited inside the holes by sputtering. To create the microhole patterning on SiO₂, the wafer was initially heated at 473 K during 10 min to remove any moisture present on the surface of the wafer. Then, the wafer was coated with ~700 nm layer of AZ 1505 photoresist (Microchemicals) by spin coating, and softbaked at 373 K during 30 s. The photoresist was illuminated with a 405 nm laser to create the pattern of holes in an area of 1 cm² using the laser lithography system, according to the design previously established in the computer controlling the system. A buffered HF solution was used as the chemical agent to remove the SiO₂ layer of the substrate in the areas not protected by the photoresist. After that, and before the remaining photoresist was removed, we coated the surface of the wafer with a 20 nm thick sputtered Ti layer. In this way, we coated the exposed surface of Si with a Ti layer acting as the metallic catalyst for the growth process of porous GaN. Finally, the photoresist was removed from the surface by using a resist stripper solution. Together with the photoresist the Ti layer deposited on the top of the photoresist was removed, while that covering the bottom of the holes and deposited on Si, remained. Figure 3 summarizes the patterning process.

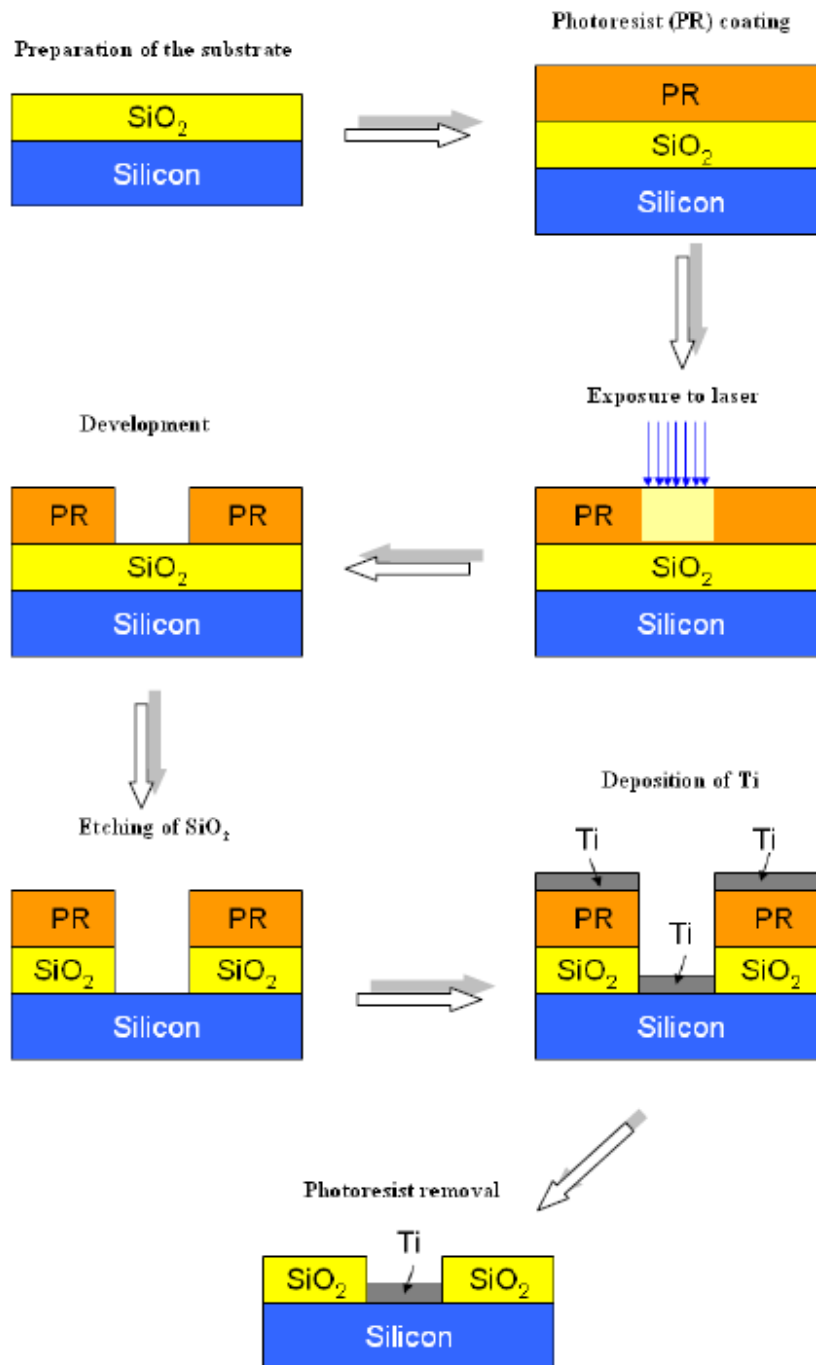


Figure 3. Scheme of the process of patterning of SiO₂ on (111) Si wafers with a 2D array of holes, 1.5 μm in diameter.

Figure 4 shows SEM images of the patterned SiO₂ on (111) Si wafers. In the image recorded with secondary electrons (see Figure 4 (a)) we can observe the array of holes, with diameters ranging from 1.4 to 1.5 μm, with a separation between holes of 2 μm, both in vertical and horizontal directions. In the image recorded with backscattered electrons (see Figure 4 (b)) we can observe that Ti, appearing with a lighter color in the image, is located only inside the holes.

These patterned substrates were coated with nanoporous GaN particles, by introducing them in the CVD system, and reducing the reaction time to 15 min to avoid overgrowth of porous GaN microparticles. As can be seen in Figure 4 (c), a well-ordered structure was obtained, covering the whole area of the patterned substrate. The growth is restricted to the patterned area, which coincides with the Ti-seeded regions. However, porous GaN was grown in the form of aggregated micron-sized nanoporous GaN particles without any preferential crystallographic orientation, as can be seen in the inset in Figure 4 (c). The XRD pattern for this sample, shown in Figure 4 (d), indicates that it does not exist any preferential growth for this samples, as it is confirmed by the homogeneous distribution of intensity in the Debye rings recorded for this sample (see inset of Figure 4(d)).

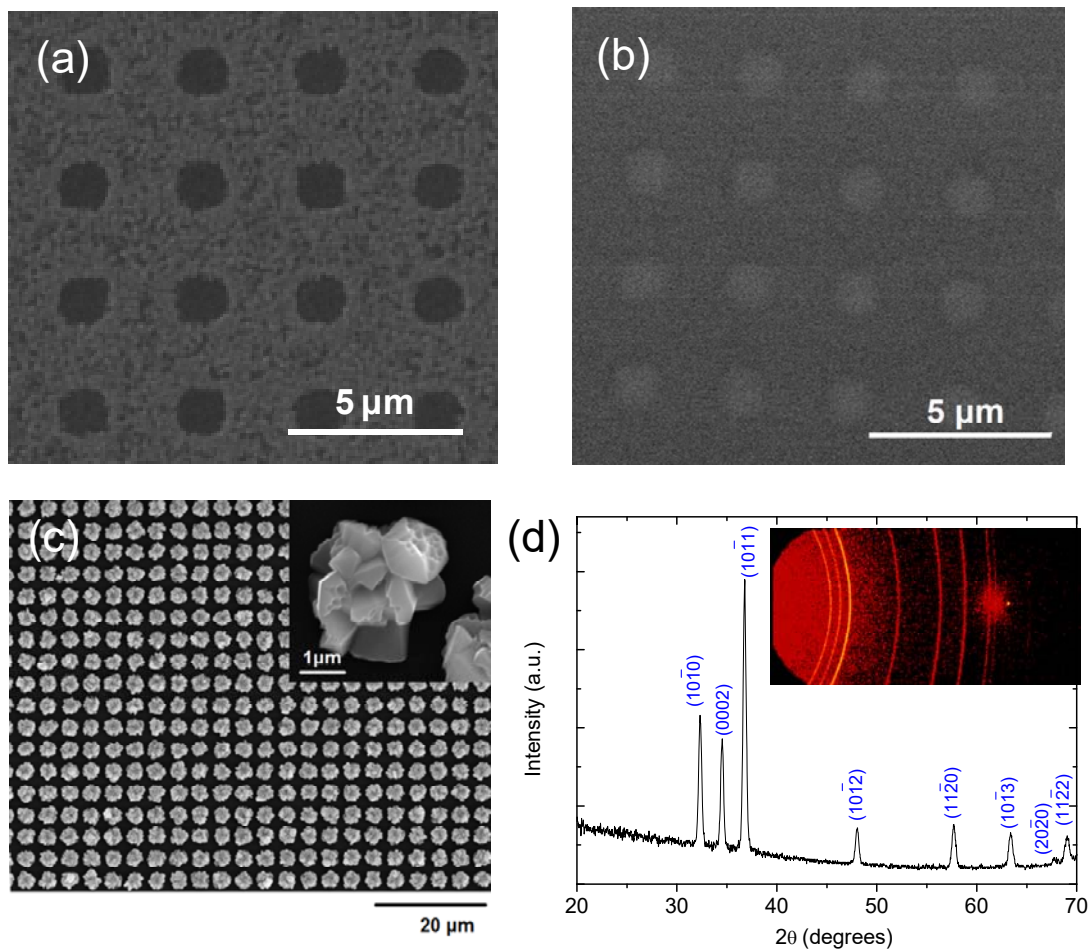


Figure 4. SEM images of the patterned SiO₂ on (111) Si substrate recorded using (a) secondary electrons and (b) backscattered electrons. (c) SEM image of the ordered porous GaN structure grown by CVD on the patterned substrates. (d) XRD pattern recorded for this structure with the corresponding Debye rings (inset).

In order to understand the lack of any preferential growth in this case, we performed additional experiments by reducing the reaction time to 12, 10 and 5 min. The results are shown in Figure 5. As can be seen from the images, at early stages, the crystal growth process starts from the edges of the microholes subsequently progressing towards its center. Thus, the crystallographic orientation of the GaN particles, expected because of

the orientational effect of the metallic catalysts, is missed due to the nucleation of the GaN particles on the SiO₂ walls of the holes, which have an amorphous structure.

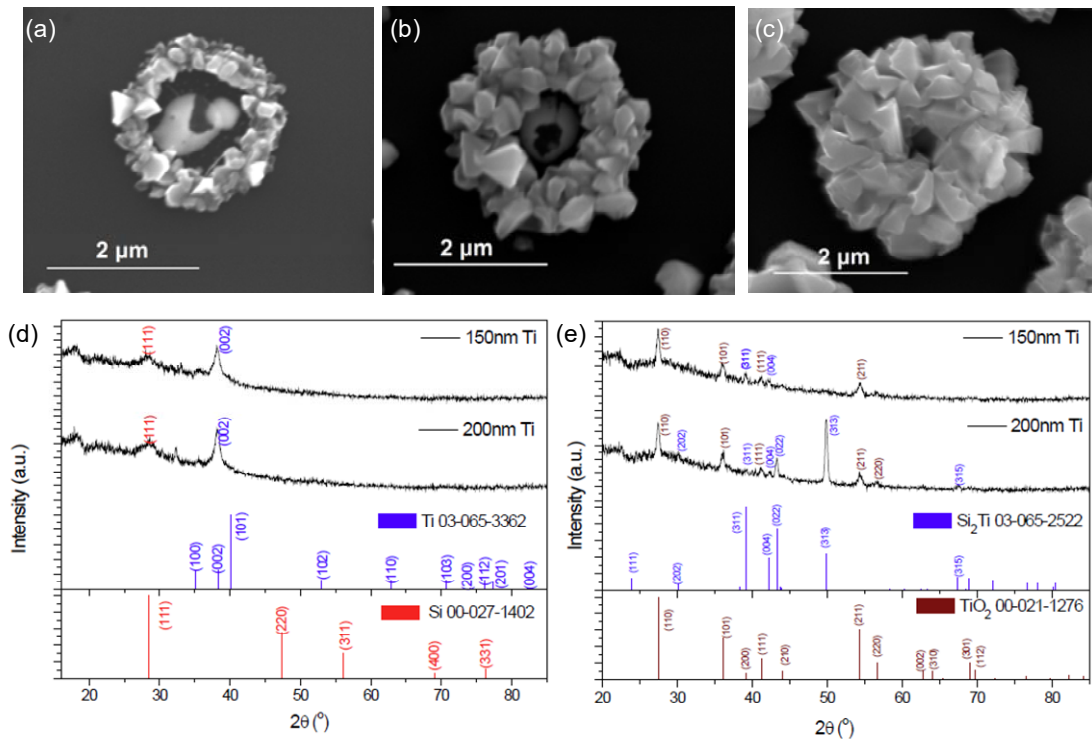


Figure 5. SEM images of porous GaN on patterned SiO₂ on (111) Si substrates at different growth stages (a) 5, (b) 10 and (c) 12 min. (d-e) XRD patterns of the SiO₂ on (111) Si substrates coated with a Ti thin film deposited by sputtering: (d) as deposited, and (e) after annealed in an NH₃ atmosphere (replicating the reaction conditions for the deposition of porous GaN by CVD).

An additional reason explaining the lack of crystallographic orientation of the porous GaN particles is that, despite the Ti thin film deposited on the SiO₂ on (111) Si substrates is oriented along the [001] direction (see Figure 5 (d)), when it is heated under the reaction conditions used for the deposition of GaN, excluding the presence of metallic Ga, Si₂Ti alloy and TiO₂ in its rutile form are formed on the surface of the sample (see Figure 5 (e)). This indicates that Ti reacts with Si, both present in the substrate and the SiO₂ coating layer, forming the Si₂Ti alloy, which the crystallographic structure (space group Fddd (03-065-2522 JCPDS file)) differs from the GaN structure. Also Ti can react with the oxygen present on the SiO₂ coating layer to form rutile, which crystallizes in the tetragonal system with space group P4₂/mnm (00-021-1276 JCPDS file).

Epitaxial growth of nanoporous GaN films

Finally, we decided to use a strategy in which no catalyst was needed for the growth of GaN films. This implied to avoid the use of metallic catalysts, and substrates with a small lattice mismatch with GaN were used. Thus, a priori, the substrate that could provide the better results would be GaN itself, since it would provide a zero lattice mismatch with the porous layer. We investigated the possibilities of obtaining an

epitaxial porous layer by using a non-porous GaN thin layer grown on a sapphire substrate (46). Non-porous GaN substrates were produced by MOCVD. The optimum results were obtained for a deposition time of 30 min, since for longer times we observed that the pores tend to coalesce, forming elongated voids, while for shorter times the thickness of the epitaxial layer is significantly reduced. Figure 6 (a) shows a SEM picture recorded at the surface of the porous layer, showing its porosity. The pores have typical diameters ranging from 200 to 300 nm; more interestingly, the walls between pores have widths ranging from 10 to 50 nm. The rocking curve corresponding to the (0004) XRD reflection of the porous GaN epitaxial layer shows a FWHM of $1508''$, similar to that of the substrate ($1540''$), indicating the good structural quality of the epitaxial porous layer (see Figure 6 (b)). Also, a shift in the position of the rocking curve is observed, indicating a slight relaxation of the porous layer when compared to the substrate, probably induced by the internal porosity.

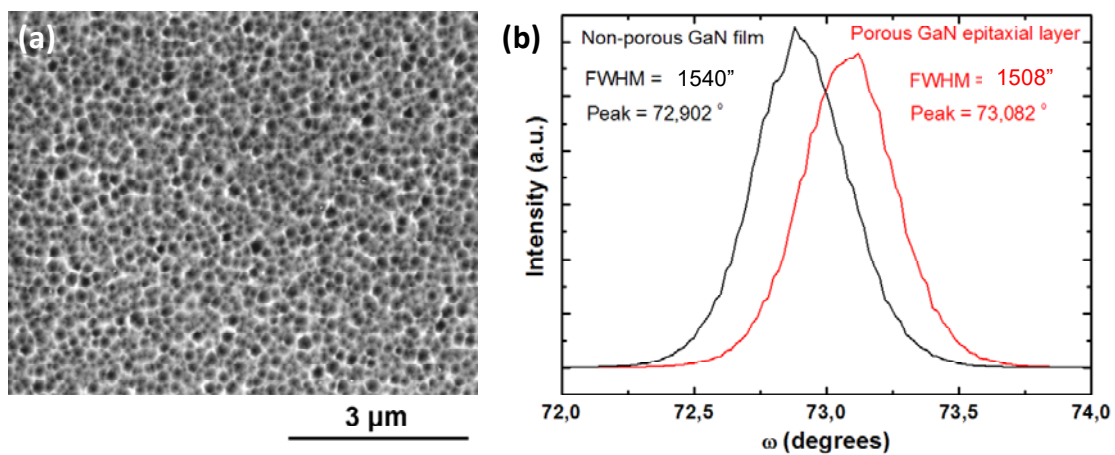


Figure 6. (a) Top view SEM image of a porous GaN epitaxial layer obtained on a non-porous GaN thin layer grown on a sapphire substrate. (b) Rocking curves of the (0004) reflection peak of the X-ray diffraction pattern recorded for the porous GaN epitaxial layer and the non-porous GaN substrate.

This allowed us to fabricate either partially or fully porous GaN diodes by CVD. Thus, *n*-type or *p*-type porous GaN epitaxial layers were deposited on non-porous GaN substrates with complementary electrical conductivity to produce partially porous GaN diodes. To produce fully porous GaN diodes by CVD, a two step synthesis process was used in which first a *n*-type or *p*-type porous GaN epitaxial layer was produced, and then, in the second step a new porous GaN epitaxial layer with complementary electrical conductivity was overgrown on the previous porous layer, as can be seen in the scheme proposed in Figure 7 (a).

The electrical characterization of these structures confirms their diode behavior, exhibiting the characteristic I-V curves with strong rectification, as can be seen in Figure 7(b). One interesting characteristic of these diodes is that the barrier to the exponential current increase is found to be in the range 0.5-0.68 V ($\sim(E_g/4q)-(E_g/2q)$) for the partially porous diodes, much lower than that reported in a non-porous GaN diode (E_g/q). This turn-on voltage is even lower in the fully porous *p-n* junctions, lying in the range $(E_g/4q) - (E_g/6q)$, resembling more the response observed in InN, GaN and other *p-n* junctions on nanowire arrays (47,48). Microscopic characterization confirmed well-defined interfaces

between the porous and the non-porous GaN (49), indicating that no significant tunneling barriers exist at either the GaN-GaN interface or the surface of the GaN/Ohmic contacts. Thus, the barrier potentials are a function of the donor and acceptor densities. A second interesting characteristic is that the current at a fixed value for the forward voltage in the fully porous diodes is found to be three orders of magnitude higher than that measured in the partially porous diodes, which would result in a more efficient system from the electrical point of view. Electron beam induced current (EBIC) measurements (see Figure 7 (c)) indicate a homogeneous carrier recombination, since contrast was only observed for the bigger pores (look at the corresponding SEM image, also included in the Figure). All these results demonstrate the good performance of the formed p-n junctions.

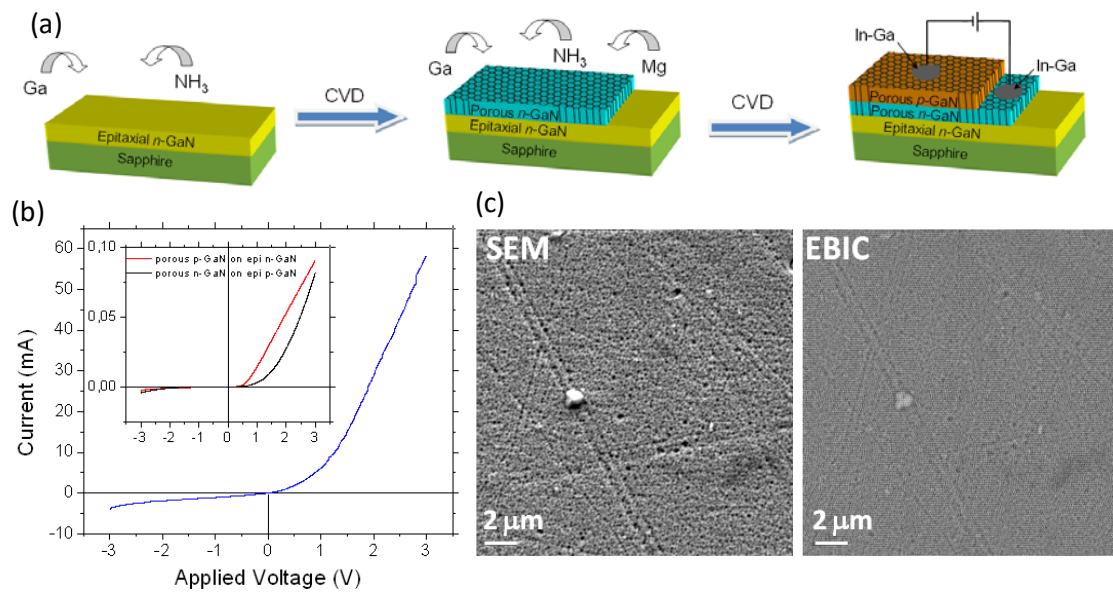


Figure 7. (a) Schematic representation of the fabrication process of fully porous GaN diodes by CVD. (b) I-V curves of the fully porous diode. The inset shows the I-V curves recorded for the partially porous diodes. (c) SEM and EBIC images of one of these diodes fabricated by CVD.

Conclusions

Taken as a whole, the investigation presented here demonstrates that partially and totally porous high quality GaN diodes can be fabricated by a CVD process, in which the lattice mismatch between the substrate and the porous GaN layer plays a crucial role, influencing both the degree of porosity and the crystallographic orientation of the porous GaN particles. We believe that this investigation can be extended to other III-N materials such as InN and AlN to span the visible spectrum, and as a route towards porous, graded index III-N materials as a basis for white light LEDs incorporating other color centers, or for improving the light extraction and narrowing the output light cone for improved LED external quantum efficiencies. High surface area diodes produced by this route do not require complicated core-shell architectures in nanostructure arrays and may be viable routes to prepare chemically stable wide bandgap (bio)sensors.

Acknowledgments

This project has been supported by the Spanish Government under Project No. MAT2013-47395-C4-4-R, and the Catalan Government under Project No. 2014SGR1358, and JCYL (VA293U13)..

References

1. V. Lehmann, U. Gösele, *Appl. Phys. Lett.*, **58**, 856 (1991).
2. I.M. Tiginyanu, V.V. Ursaki, E. Monaco, E. Foca, H. Föll, *Electrochem. Solid-State Lett.*, **10**, D127 (2007).
3. C. O'Dwyer, D.N. Buckley, D. Sutton, M. Serantoni, S.B. Newcomb, *J. Electrochem. Soc.*, **154**, H78 (2007).
4. M.A. Steven-Kalceff, I.M. Tiginyanu, S. Langa, H. Föll, H.L. Hartnagel, *J. Appl. Phys.*, **89**, 2560 (2001).
5. D. Kovalev, V.Y. Timoshenko, N. Künzner, E. Gross, F. Koch, *Phys. Rev. Lett.*, **87**, 068301 (2001).
6. V. Kochergin, *Omnidirectional Optical Filters*, Kluwer Academic, Boston (2003).
7. V. Kovalev, G. Polisski, J. Diener, H. Heckler, N. Künzner, V.Y. Timoshenko, F. Koch, *Appl. Phys. Lett.*, **78**, 916 (2001).
8. V. Kochergin, M. Christophersen, P.R. Swinehart, *Proc. SPIE*, **5554**, 223 (2004).
9. G. Kaltsas, A.G. Nassiopoulou, *Sens. Actuators A*, **76**, 133 (1999).
10. C.J. Oton, L. Pancheri, Z. Gaburro, L. Pavesi, C. Baratto, G. Faglia, G. Sberveglieri, *Phys. Status Solidi A*, **197**, 523 (2003).
11. Y. Huang, X. Duan, Y. Cui, C.M. Lieber, *Nano Lett.*, **2**, 101 (2002).
12. S. Nakamura, M.R. Krames, *Proc. IEEE*, **101**, 2211 (2013).
13. S.C. Jain, M. Willander, J. Narayan, R.V. Overstraeten, *J. Appl. Phys.*, **87**, 965 (2000).
14. H. Shibata, Y. Waseda, H. Ohta, K. Kiyomi, K. Shimoyama, K. Fujito, H. Nagaoka, Y. Kagamitani, R. Simura, T. Fukuda, *Mater. Trans.*, **48**, 2782 (2007).
15. T. Palacios, A. Chakraborty, S. Rajan, C. Poblenz, S. Keller, S.P. DenBaars, J.S. Speck, U.K. Mishra, *IEEE Electron Device Lett.*, **26**, 781 (2005).
16. M. Leszczynski, H. Teisseyre, T. Suski, I. Grzegory, M. Bockowski, J. Jun, S. Porowski, K. Pakula, J.M. Baranowski, C.T. Foxon, T.S. Cheng, *Appl. Phys. Lett.*, **69**, 73 (1996).
17. R. Dahal, B. Pantha, J. Li, J.Y. Lin, H.X. Jiang, *Appl. Phys. Lett.*, **94**, 063505 (2009).
18. C.J. Neufeld, N.G. Toledo, S.C. Cruz, M. Iza, S.P. DenBaars, U.K. Mishra, *Appl. Phys. Lett.*, **93**, 143502 (2008).
19. S. Strite, H. Morkoç, *J. Vac. Sci. Technol. B*, **10**, 1237 (1992).
20. M. Mynbaeva, N. Bazhenov, K. Mynbaev, V. Evstropov, S.E. Saddow, Y. Koshka, Y. Melnik, *Phys. Status Solidi B*, **228**, 589 (2001).
21. M. Mynbaeva, A. Titkov, A. Kryganovskii, V. Ratnikov, K. Mynbaev, H. Huhtinen, R. Laiho, V. Dmitriev, *Appl. Phys. Lett.*, **76**, 1113 (2000).
22. X. Li, Y.W. Kim, P.W. Bohn, I. Adesida, *Appl. Phys. Lett.*, **80**, 980 (2002).

23. A.P. Vajpeyi, S.J. Chua, S. Tripathy, E.A. Fitzgerald, W. Liu, P. Chen, L.S. Wang, *Electrochem. Solid-State Lett.*, **8**, G85 (2005).
24. M. Ohkubo, *J. Cryst. Growth*, **189-190**, 734 (1998).
25. D.J. Díaz, T.L. Williamson, I. Adesida, P.W. Bohn, R.J. Molnar, *J. Appl. Phys.*, **94**, 7526 (2003).
26. C. Youtsey, I. Adesida, G. Bulman, *Appl. Phys. Lett.*, **71**, 2151 (1997).
27. M. Ainorkhilah, A. Naser Mahmoud, Y. Yuhamdan, F.K. Yam, L.S. Chuah, R.A. Husnen, H. Zainuriah, *Int. J. Electrochem. Sci.*, **8**, 5801 (2013).
28. C.B. Soh, H. Hartono, S.Y. Chow, S.J. Chua, E.A. Fitzgerald, *Appl. Phys. Lett.*, **90**, 053112 (2007).
29. Y. Zhang, B. Leung, J. Han, *Appl. Phys. Lett.*, **100**, 181908 (2012).
30. A. Ramizy, Z. Hassan, K. Omar, *Sens. Actuators B*, **155**, 699 (2011).
31. F.K. Yam, Z. Hassan, *Appl. Surf. Sci.*, **253**, 9525 (2007).
32. J.J. Wierer, A. David, M.M. Megens, *Nat. Photon.*, **3**, 163 (2009).
33. J.C. Vial, A. Bsiesy, F. Gaspard, R. Herino, M. Ligeon, F. Müller, R. Romestain, R.M. Macfarlane, *Phys. Rev. B*, **45**, 14171 (1992).
34. J.M. Hwang, W.H. Hung, H.L. Hwang, *IEEE Photon. Technol. Lett.*, **20**, 608 (2008).
35. R. Wang, D. Liu, Z. Zuo, Q. Yu, Z. Feng, X. Xu, *AIP Adv.*, **2**, 012109 (2012).
36. K. Kim, J. Choi, T.S. Bae, M. Jung, D.H. Woo, *Jpn. J. Appl. Phys.*, **46**, 6682 (2007).
37. S.W. Ryu, J. Park, J.K. Oh, D.H. Long, K.W. Kwon, Y.H. Kim, J.K. Lee, J.H. Kim, *Adv. Funct. Mater.*, **19**, 1650 (2009).
38. C.Y. Cho, S.E. Kang, K.S. Kim, S.J. Lee, Y.S. Choi, S.H. Han, G.Y. Jung, S.J. Park, *Appl. Phys. Lett.*, **96**, 181110 (2010).
39. S. Chhajed, W. Lee, J. Cho, E.F. Schubert, J.K. Kin, *Appl. Phys. Lett.*, **98**, 071102 (2011).
40. X. Fu, B. Zhang, X. Kang, J. Deng, C. Xiong, T. Dai, X. Jiang, T. Yu, Z. Chen, G.Y. Zhang, *Opt. Express*, **19**, A1104 (2011).
41. J.J. Carvajal, J.C. Rojo, *Cryst. Growth Des.*, **9**, 320 (2009).
42. J.J. Carvajal, O.V. Bilousov, D. Drouin, M. Aguiló, F. Díaz, J.C. Rojo, *Microsc. Microanal.*, **18**, 905 (2012).
43. M.M. Sung, C.Kim, S.H. Yoo, C.G. Kim, Y. Kim, *Chem. Vap. Deposition*, **8**, 50 (2002).
44. O.V. Bilousov, J.J. Carvajal, D. Drouin, X. Mateos, F. Díaz, M. Aguiló, C. O'Dwyer, *ACS Appl. Mater. Interfaces*, **4**, 6927 (2012).
45. J.H. Choi, A. Zoukarnneev, S.I. Kim, C.W. Baik, M.H. Yang, S.S. Park, H. Suh, U.J. Kim, H.B. Son, J.S. Lee, M. Kim, J.M. Kim, K. Kim, *Nat. Photon.*, **5**, 763 (2011).
46. O.V. Bilousov, J.J. Carvajal, J. Mena, O. Martínez, J. Jiménez, H. Geaney, F. Díaz, M. Aguiló, C. O'Dwyer, *CrystEngComm*, **16**, 10255 (2014).
47. J.R. Kim, H. Oh, H.M. So, J. Kim, J.J. Kim, *Physica E*, **18**, 225 (2003).
48. G. Cheng, A. Kolmakov, Y. Zhang, O. Moskovits, R. Munden, M.A. Reed, G. Wang, D. Moses, J. Zhang, *Appl. Phys. Lett.*, **83**
49. O.V. Bilousov, J.J. Carvajal, H. Geaney, V.Z. Zubialevich, P.J. Parbrook, O. Martínez, J. Jiménez, F. Díaz, M. Aguiló, C. O'Dwyer, *ACS Appl. Mater. Interfaces*, **6**, 17954 (2014).